ChemPubSoc Europe

DOI: 10.1002/chem.201706075

CHEMISTRY A European Journal Full Paper

Nucleophilic Substitution Reactions

Nucleophilic Substitution in Solution: Activation Strain Analysis of Weak and Strong Solvent Effects

Trevor A. Hamlin,[a] Bas van Beek,[a] Lando P. Wolters,[a] and F. Matthias Bickelhaupt*[a, b]

Abstract: We have quantum chemically studied the effect of various polar and apolar solvents on the shape of the potential energy surface (PES) of a diverse collection of archetypal nucleophilic substitution reactions at carbon, silicon, phosphorus, and arsenic by using density functional theory at the OLYP/TZ2P level. In the gas phase, all our model S_N2 reactions have single-well PESs, except for the nucleophilic substitution reaction at carbon (S_N2@C), which has a double-well energy profile. The presence of the solvent can have a significant effect on the shape of the PES and, thus, on the nature of the S_N2 process. Solvation energies, charges on the nucleophile or leaving group, and structural features are compared for the various S_N2 reactions in a spectrum of solvents. We demonstrate how solvation can change the shape of the PES, depending not only on the polarity of the solvent, but also on how the charge is distributed over the interacting molecular moieties during different stages of the reaction. In the case of a nucleophilic substitution at three-coordinate phosphorus, the reaction can be made to proceed through a single-well [no transition state (TS)], bimodal barrier (two TSs), and then through a unimodal transition state (one TS) simply by increasing the polarity of the solvent.

Introduction

The bimolecular nucleophilic substitution (S_N2) is one of the most studied and widely recognized elementary chemical reactions in organic chemistry; a typical example is shown in Scheme 1 for A = carbon, with chloride as nucleophile and leaving group.[1] This reaction type has recently been reviewed[2] and has been the subject of an exceptional number of experimental[3] and theoretical[4] studies over the past 70 years. In archetype S_N2 processes, at least one charged species is present before and/or after the elementary reaction step. Often, such species react in a very different manner in the gas phase when compared to the solution phase, due to substantial stabilization of the charged species by the solvent. Hence, the behavior and rate of this reaction is contingent on the medium in which the reaction is conducted.[3f,5]

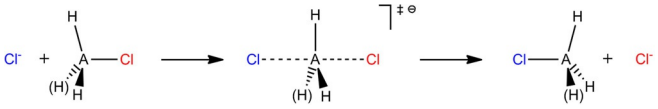

Scheme 1. Model S_N2 reactions at A = C, Si, P, or As.

The bimolecular nucleophilic substitution at carbon (S_N2@C: see Scheme 1, A = C) proceeds through a backside attack of the Cl^- nucleophile at the carbon atom, followed by a concerted expulsion of the Cl^- leaving group. In the gas phase, this process occurs through a double-well potential energy surface (PES) and a reactant and product complex (RC and PC, respectively) are separated by a pentacoordinate transition state (TS) (see Figure 1 b).[3,4] Solvation in aqueous solution transforms this double-well PES to a unimodal PES (see Figure 1 c).[3,4] The mechanism behind this drastic solvent effect on the reaction profile is explained by differential solvation of the reactants, products, intermediates, and transition states.[6]

The overall structural transformation for a bimolecular nucleophilic substitution at silicon[7] and phosphorus[8] (S_N2@Si and S_N2@P, respectively: see Scheme 1, A = Si and A = P, respectively) is equivalent to that of S_N2@C, however, the potential energy surface is noticeably different. Our understanding of the effect of solvation on these reactions is much less explored and as a result less concrete. What we do know is that in the gas phase, S_N2@Si and S_N2@P reactions proceed through a single-well PES associated with a D_{3h} symmetric transition complex (TC), thereby proceeding without encountering a first-order saddle point (see Figure 1 a). Aqueous solvation destabil-

[a] Dr. T. A. Hamlin, B. van Beek, Dr. L. P. Wolters, Prof. Dr. F. M. Bickelhaupt
Department of Theoretical Chemistry
Amsterdam Center for Multiscale Modeling (ACMM)
Vrije Universiteit Amsterdam
De Boelelaan 1083, 1081 HV Amsterdam (The Netherlands)
E-mail: f.m.bickelhaupt@vu.nl

[b] Prof. Dr. F. M. Bickelhaupt
Institute of Molecules and Materials (IMM)
Radboud University Nijmegen
Heyendaalseweg 135, 6525 AJ Nijmegen (The Netherlands)

Supporting information [containing the COSMO settings (including the atomic radii), additional plots, Cartesian coordinates, structures, and energies of all stationary points] and the ORCID number(s) for the author(s) of this article can be found under https://doi.org/10.1002/chem.201706075.

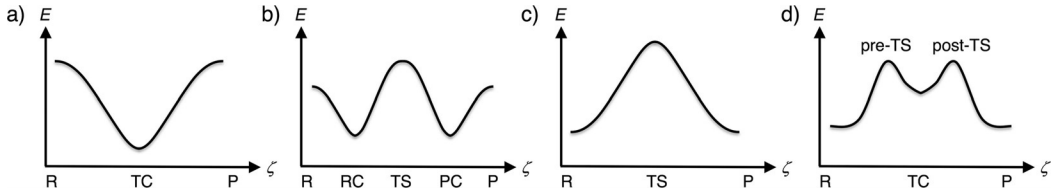

Figure 1. Typical reaction profiles [energy (E) vs. reaction coordinate (ζ)]. a) Single-well, b) double-well, c) unimodal barrier, and d) bimodal barrier. R = reactants, RC = reactant complex, TS = transition state, TC = transition complex, pre-TS = transition state leading to the TC, post-TS = transition state leading away from the TC, PC = product complex, P = products.

izes the transition complex for S_N2@Si and S_N2@P reactions and turns the PESs into unimodal reaction profiles, with central transition states (see Figure 1 c).[7b]

Bimolecular nucleophilic substitution at arsenic (S_N2@As: see Scheme 1, A = As) is even far less investigated and is included in the present study due to its chemical (valence isoelectronic) similarity to phosphorus, appearing just below arsenic on the periodic table. Arsenic has both a near identical electronegativity and atomic radius to phosphorus.[9] Additionally, in biological systems, arsenic is thought to behave similarly to phosphorus.[10] It has been proposed that in the presence of arsenate, a strain of *Halomonas* bacteria (GFAJ-1) could incorporate arsenic into the backbone of DNA in competition with phosphorus.[11] Auxiliary investigations, however, revealed that arsenate does not allow for incorporation of arsenic into *Halomonas* DNA when phosphate is limiting.[12] The arsenate-ester hydrolysis reaction (S_N2@As4) has been studied computationally by Šponer et al. and they calculated a bimodal barrier for the reaction in the gas phase and in water.[13] Furthermore, systematically modeling S_N2@As adds an extra dimension to the more fundamental interest in investigating the shape of the PESs for nucleophilic substitution reactions at arsenic and how they compare to the other electrophilic centers.

Intrigued by the intricacies of solvation on the nature and rate of S_N2 reactions, we have quantum chemically explored and analyzed the PESs of nucleophilic substitutions at various electrophilic centers and in a spectrum of solvents. The objective of the current research is to understand these fundamental processes in a variety of solvents. This is relevant for a wide range of disciplines, including organic, inorganic, (exo)planetary, and biological chemistry. For example, understanding how S_N2@P changes in various solvents has direct implications for the backbone elongation concomitant with DNA replication and is a continuation of our ongoing research line into DNA stabilization and replication.[14] Additionally, there have been many potential solvents discovered in our solar system to date in various forms, either liquid, icy mixtures, gas, or transiently.[15] Understanding how solvent polarity affects the kinetics and the overall shape of the PES for archetypical nucleophilic substitution reactions on Earth as well as elsewhere in the cosmos has intrinsic value. A comprehensive analysis on the effect of systematically varying solvent polarity on S_N2 substitution reactions at different electrophilic centers has, to the best of our knowledge, not yet been carried out.

Theoretical Methods

Computational details

The density functional theory (DFT)[16]-based quantum chemical calculations were carried out by using the Amsterdam density functional (ADF 2014.01) program.[17] A generalized gradient approximation (GGA) of DFT by using the OLYP functional was selected for the calculations. This GGA functional utilizes the optimized exchange (OPTX) functional proposed by Handy and co-workers,[18] and the Lee–Yang–Parr (LYP) correlation functional.[19] This exchange and correlation functional reproduces S_N2@C and S_N2@Si barriers within a few kcal mol^{-1} compared to highly correlated ab initio benchmarks,[4n,7c] providing sufficient accuracy to study the qualitative effects on the PES shapes upon varying the solvent polarity. Vibrational analysis confirmed energy minima (no imaginary frequencies) and transition states (a single imaginary frequency). The all-electron TZ2P basis set used herein is of triple-ζ quality and consists of a large uncontracted set of Slater-type orbitals used to construct the molecular orbitals (MOs). The basis set has been augmented with two sets of polarization functions, that is, 2p and 3d on hydrogen, 3d and 4f on carbon, oxygen, silicon, phosphorus, and chlorine. The accuracy parameter of both the Becke grid integration and the Zlm fit scheme were set to EXCELLENT.[20]

All solution-phase calculations employ COSMO to simulate solvent effects.[21] Seven solvents in the range $\varepsilon_r = [2.4, 188.4]$ were considered to emulate a wide spectrum of solvents. The relative dielectric constants ε_r of toluene, chloroform, ammonia, methanol, water, formamide, and methylformamide are 2.4, 4.8, 16.9, 32.6, 78.4, 109.5, and 188.4, respectively. Default parameters in ADF were used for all solvents except for water. In the case of water, the solvent radius (R_s) was taken from experimental data for the macroscopic density (ρ) and the molecular mass (M_m) with the formula $R_s^3 = 2.6752 M_m \rho^{-1}$, leading to an R_s value of 1.9 Å for water. Atomic radii values were taken from the MM3 van der Waals radii,[22] and scaled by 0.8333 (the MM3 radii are 20% larger than the normal van der Waals radii due to the specific form of the van der Waals energy within the MM3 force field). The surface charges at the GEPOL93 solvent-excluding surface[23] were corrected for outlying charges. This setup provides a "non-empirical" approach to including solvent effects with a dielectric continuum and works well for solvation processes, accurately reproducing experimental hydration energies of the chloride ion.[24] A sample ADF input file involving a geometry optimization in water is provided in the Supporting Information.

Activation strain model

The activation strain model (ASM), also known as distortion/interaction model, is a useful tool for investigating the factors giving rise to activation barriers.[25] The activation barrier, or well, results

from the interplay between the strain energy (ΔE_{strain}) and the interaction energy (ΔE_{int}) [Eq. (1)].

$$\Delta E = \Delta E_{strain} + \Delta E_{int} \quad (1)$$

The transition structure is separated into two fragments (the distorted substrate and the chloride ion), followed by single-point energy calculations on each fragment. The difference in energy between the optimized ground-state structure and the distorted structures is the strain energy (ΔE_{strain}), whereas ΔE_{int} refers to the interaction between the deformed reactants.

Furthermore, the ASM model has been extended to account for solvation, which is in line with previous work by De Cózar and coworkers.[4e] In this framework, the $\Delta E_{solution}$ (PES in solution) is decomposed into the energy of the solute (ΔE_{solute}), specifically the reaction system in vacuum with the solution-phase geometry, plus the solvation energy ($\Delta E_{solvation}$) [Eq. (2)].

$$\Delta E_{solution} = \Delta E_{solute} + \Delta E_{solvation} \quad (2)$$

ΔE_{strain} and ΔE_{int} make up the intrinsic energy of the solute (ΔE_{solute}) and are augmented by the solvation term $\Delta E_{solvation}$, as shown in Equation (3).

$$\Delta E_{solution} = \Delta E_{strain} + \Delta E_{int} + \Delta E_{solvation} \quad (3)$$

Notably, ΔE_{strain} and ΔE_{int} refer to the strain of, and mutual interaction between, the solute reactant molecules in their solution geometries, but in the absence of the solvent. As such, the strain is computed as the energy difference between the solute reaction system relative to the solute reactants in vacuum. The $\Delta E_{solvation}$ term accounts for interaction of the solute with both the solvent and the cavitation, that is, the formation of a cavity in the solvent by the presence of the solute. This approach to extending upon the ASM differs from a prior approach,[26] in which all solvent effects were incorporated in either the strain or interaction terms.

Results and Discussion

The results of our OLYP/TZ2P calculations in the gas phase and seven selected solvents are presented in Tables 1 and 2 as well as in Figure 2. Reaction profiles for the S_N2@C, S_N2@Si, and S_N2@P reactions in the gas and aqueous phase provided here are, where available, in line with previous studies.[7b] Driven to assess the effect of solvation on the shape of the PES and to provide new insights into the backside S_N2 reaction mechanism, we systematically screened solvents of varying polarity. We observe dramatic variation in the shape of the PES in the range of vacuum to ammonia, followed by minimal deviations for polar solvents with dielectric constants greater than $\varepsilon_r = 16.9$ (ammonia). In addition, we find that an increase in the solvent polarity results in destabilization of the transition zone and rising of energy barriers. Under strongly polar conditions, the PES eventually becomes unimodal for S_N2@C, S_N2@P3, and S_N2@P4 reactions and bimodal for S_N2@Si and S_N2@As4 reactions.

Nucleophilic substitution at carbon

The first reaction we discuss is $Cl^- + CH_3Cl$ (S_N2@C, Table 1, entries 1 a–h, Figure 2 a). The PES for S_N2@C shifts from a double-well in the gas phase, as well as in non-polar solvents, to unimodal as the solvent polarity increases. Specifically, the PES is characterized by a double-well in vacuum, toluene, and chloroform, having a reactant complex that becomes less stabilized relative to the reactants as the polarity increases, which is in line with previous observations by Chandrasekhar et al.[4m] Thus, the energy of the reactant and product complexes (RC and PC, respectively) at the bottom of the double-well relative to the separate reactants and products (R and P, respectively) increases from −9.1, −2.6, to −1.0 kcal mol^{-1} (Table 1, entries 1 a–c). The central barrier associated with reaching the D_{3h}-symmetric transition state (TS) rises significantly as the polarity increases. Initially, there is a slightly negative barrier of −0.1 kcal mol^{-1} in the gas phase and the barrier rises to 22.7 kcal mol^{-1} in the most polar solvent, that is, methylformamide. A significant change in the PES is observed in ammonia, as the double-well transforms to a unimodal barrier with the reactant complex (RC) disappearing. This unimodal barrier persists in ammonia and more polar solvents and it coalesces with the $\Delta\Delta E_{TS}$ varying only by 1.2 kcal mol^{-1}. The $\Delta\Delta E_{TS}$ is greatest (13.3 kcal mol^{-1}) when changing from vacuum to toluene despite the fact that the $\Delta\varepsilon$ between vacuum and toluene is only 2.4. This reveals that a modest change in the solvent polarity compared to vacuum has a drastic effect on the shape of the PES, which indeed appears to be the case for all S_N2 reactions studied herein.

Nucleophilic substitution at silicon

The energetics of the reaction $Cl^- + SiH_3Cl$ (S_N2@Si, Table 1, entries 2 a–h, Figure 2 b) are discussed next. The pentavalent [Cl-SiH_3-Cl]$^-$ is a stable energy minimum, referred to as transition complex (TC), at variance with the labile transition state (TS) discussed for S_N2@C above. As the polarity increases from the gas phase to chloroform, the single-well PES becomes increasingly shallow (Table 1, entries 2 a–c). Unlike for S_N2@C, the PES for S_N2@Si in ammonia, turns into a bimodal barrier with a C_{3v}-symmetric pre-transition state (pre-TS) that is slightly higher (0.1–0.2 kcal mol^{-1}) in energy than the D_{3h}-symmetric TC (Table 1, entries 2 d–h). In a previous communication from our group, it was reported that S_N2@Si in water proceeds through a unimodal barrier, which, because of a numerical artifact, experienced a shift in the transition vector to a slightly positive value (38 cm^{-1}).[7b] This may be an incomplete view of the surface topology because when using the highest quality numerical integration scheme and careful analysis, a bimodal barrier emerges. Note, however, that the PES around the transition complex is extremely shallow and locating the pre-TS complexes proved non-trivial. The activation barrier for S_N2@Si is significantly lower than for S_N2@C, by approximately 18 kcal mol^{-1}, and increases monotonically from 3.1 to 4.5 kcal mol^{-1} when moving from ammonia to methylformamide (Table 1, entries 2 d–h).

Nucleophilic substitution at phosphorus

The shape of the PES for S_N2@P3 $Cl^- + PH_2Cl$ varies significantly based on the solvent polarity. A single-well exists in vacuum, toluene, and chloroform that becomes increasingly shallow, in

Table 1. Energies (in [kcal mol^{-1}]) relative to the reactants of stationary points along the PES of the symmetric S_N2 reactions in the gas phase and in solution.[a]

No.	Medium[b]	Reaction[c]	Shape of the PES[d]	Reactant complex/(pre-transition state) ΔE_{RC} ($\Delta E_{p\text{-}TS}$)	Transition state/(transition complex) ΔE_{TS} (ΔE_{TC})
1a	gas	$Cl^- + CH_3Cl$	double-well	−9.1	−0.1
1b	toluene		double-well	−2.6	13.2
1c	chloroform		double-well	−1.0	18.0
1d	ammonia		unimodal	–	21.5
1e	methanol		unimodal	–	21.9
1f	water		unimodal	–	22.1
1g	formamide		unimodal	–	22.6
1h	methylformamide		unimodal	–	22.7
2a	gas	$Cl^- + SiH_3Cl$	single-well	–	(−24.3)
2b	toluene		single-well	–	(−7.7)
2c	chloroform		single-well	–	(−1.6)
2d	ammonia		bimodal	(3.1)	(2.9)
2e	methanol		bimodal	(3.8)	(3.7)
2f	water		bimodal	(3.9)	(3.8)
2g	formamide		bimodal	(4.4)	(4.3)
2h	methylformamide		bimodal	(4.5)	(4.4)
3a	gas	$Cl^- + PH_2Cl$	single-well	–	(−26.0)
3b	toluene		single-well	–	(−9.9)
3c	chloroform		single-well	–	(−4.0)
3d	ammonia		bimodal	(0.9)	(0.3)
3e	methanol		bimodal	(1.4)	(1.1)
3f	water		unimodal	–	1.2
3g	formamide		unimodal	–	1.7
3h	methylformamide		unimodal	–	1.8
4a	gas	$Cl^- + POH_2Cl$	single-well	–	(−22.3)
4b	toluene		single-well	–	(−4.0)
4c	chloroform		unimodal	–	2.9
4d	ammonia		unimodal	–	7.9
4e	methanol		unimodal	–	8.8
4f	water		unimodal	–	8.9
4g	formamide		unimodal	–	9.6
4h	methylformamide		unimodal	–	9.7
5a	gas	$Cl^- + AsH_2Cl$	single-well	–	(−29.6)
5b	toluene		single-well	–	(−13.2)
5c	chloroform		single-well	–	(−7.1)
5d	ammonia		single-well	–	(−2.6)
5e	methanol		single-well	–	(−1.8)
5f	water		single-well	–	(−1.7)
5g	formamide		single-well	–	(−1.2)
5h	methylformamide		single-well	–	(−1.1)
6a	gas	$Cl^- + AsOH_2Cl$	single-well	–	(−29.6)
6b	toluene		single-well	–	(−10.7)
6c	chloroform		single-well	–	(−3.6)
6d	ammonia		bimodal	(1.8)	(1.6)
6e	methanol		bimodal	(2.7)	(2.6)
6f	water		bimodal	(2.9)	(2.7)
6g	formamide		bimodal	(3.4)	(3.3)
6h	methylformamide		bimodal	(3.8)	(3.5)

[a] Computed at the OLYP/TZ2P level. [b] Solvent modeled with COSMO. [c] See the Supporting Information for structures and Cartesian coordinates. [d] See Figure 2 for PESs.

a systematic manner, ranging from −26.0 to −4.0 kcal mol^{-1} (Table 1, entries 3a–c, Figure 2c). In ammonia and methanol, the shape of the PES transforms into a bimodal barrier (Table 1, entries 3d and e). Gilheany and co-workers also observed a bimodal barrier for S_N2@P depending on the solvent polarity by using NMR spectroscopic and computational techniques.[8c] Extremely low barriers of 0.9–1.4 kcal mol^{-1} associated with this pre-TS lead to a slightly more stable (0.3–0.6 kcal mol^{-1}) pentacoordinate TC, similar to the case of S_N2@Si in solution when $\varepsilon_r \geq 16.9$. Solvation in water and more polar solvents results in a unimodal PES (Table 1, entries 3f–h). The pre-TS no longer exists in these solvents and instead, a C_{2v}-symmetric TS associated with very low activation barriers ranging from 1.2 to 1.7 and 1.8 kcal mol^{-1} is observed, in water, formamide, and methylformamide, respectively (Figure 2c). In short, by increasing the polarity of the solvent for S_N2@P3, we recover both the shift from a single-well PES to a bimodal PES that was observed for S_N2@Si, and, continuing along the spectrum, the shift from a bimodal PES to a unimodal PES, similar to S_N2@C.

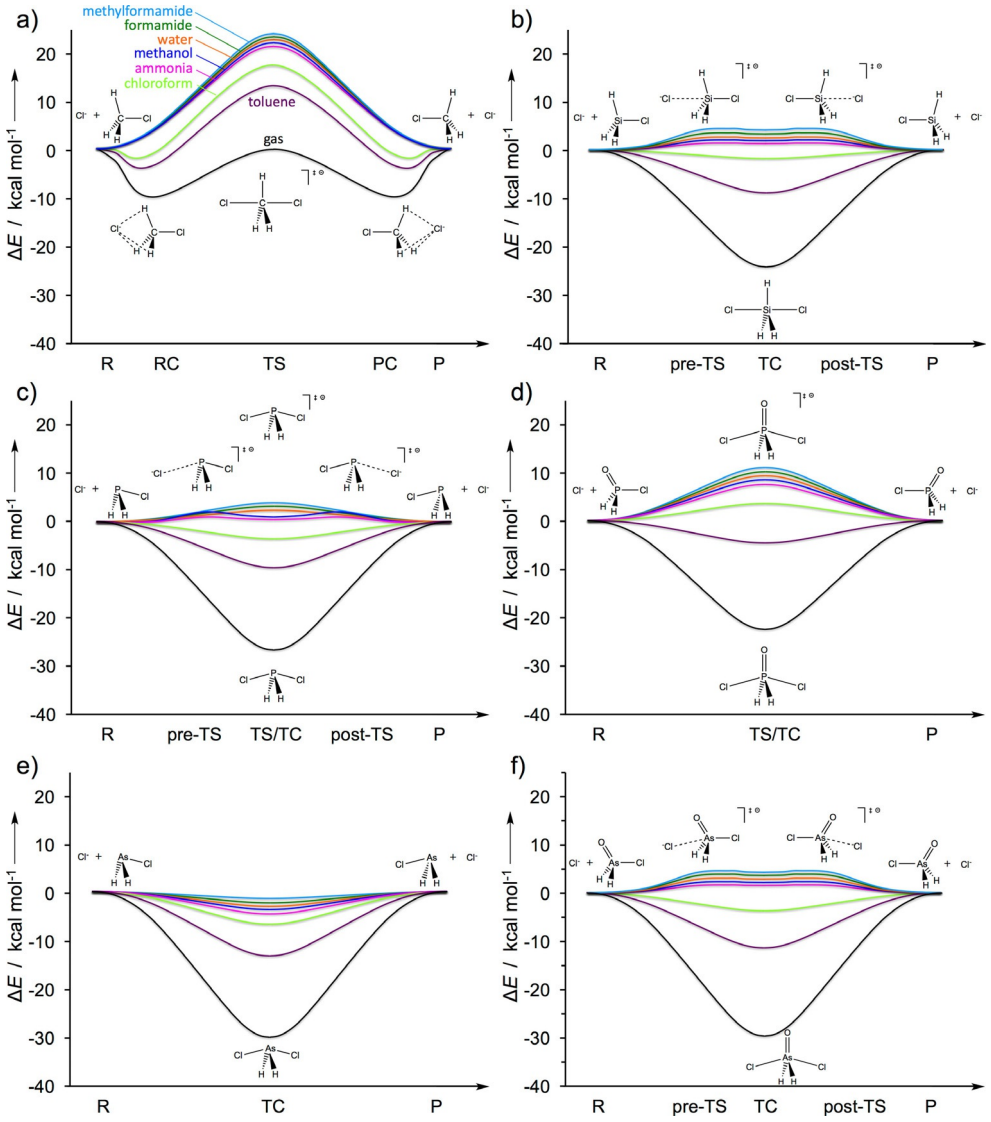

Figure 2. Reaction profiles of six S_N2 reactions. a) S_N2@C, b) S_N2@Si, c) S_N2@P3, d) S_N2@P4, e) S_N2@As3, and f) S_N2@As4, computed at the OLYP/TZ2P level by using COSMO to simulate the effect of solvation. In each case, the order of the solvents remains the same, varying systematically from least polar to most polar.

In the case of the S_N2@P4 reaction $Cl^- + POH_2Cl$, we find that the transition structures (either transition state or transition complex) are destabilized by 4–8 kcal mol^{-1} compared to the S_N2@P3 reaction $Cl^- + PH_2Cl$, due to an increased coordination at the electrophilic center.[7b] We discuss the effect of increased coordination and the resulting effects it has on both the interaction and the strain energy below in the Activation Strain Analysis section. In vacuum and toluene, S_N2@P4 occurs through a single-well (Table 1, entries 4a and b, Figure 2d). Moving to chloroform and the other polar solvents, the PES shifts directly to a unimodal barrier, with a C_{2v}-symmetric TS (Table 1, entries 4c–h). The bimodal PES is bypassed in this oxide system compared to the non-oxide substrate (compare Figures 2c and d). The barriers for S_N2@P4 rise incrementally in ammonia and more polar solvents and vary from 7.9 to 9.7 kcal mol^{-1} (Table 1, entries 4d–h).

Nucleophilic substitution at arsenic

The PES associated with the S_N2@As3 reactions deviates significantly from the PES for S_N2@P3 in ammonia and more polar solvents. This is the only S_N2 reaction included in the present study that does not have a barrier even in the most polar of solvents. A single-well PES is observed for S_N2@As3 in every solvent (Table 1, entries 5a–h) and is deepest for the reaction in the gas phase (−29.6 kcal mol^{-1}). From the gas phase to solvation, and going to more polar solvents, we recover the same trend of a decreasing stability of the transition complex as we found for the other reactions, that is, the single-well becomes increasingly shallow in a monotonic fashion as the solvent polarity increases, to a final ΔE_{TC} of −1.1 kcal mol^{-1} in methylformamide (Table 1, entry 5h).

The PES for S_N2@As4 is a single-well in the gas phase and in the non-polar solvents, toluene and chloroform, with the stabi-

lization of the TC relative to the reactants R varying greatly from −29.6 to −10.7 to −3.6 kcal mol^{-1}, respectively (Table 1, entries 6a–c). When transitioning to ammonia and increasingly polar solvents, the PES shifts to a bimodal barrier with a C_{2v}-symmetric TC (Table 1, entries 6d–h). The bimodal PES has a C_s-symmetric pre-TS and post-TS that connect the separated reactants/products and the TC. The pre-TS and post-TS are similar in shape to those occurring in the S_N2@Si reaction. The transition structures (pre-TS, TC, TS, and post-TS) for S_N2@As4 are all destabilized compared to the non-oxide (S_N2@As3) variants by 0–4 kcal mol^{-1}. This relative destabilization caused by the oxide functionality is less extreme than was the case for S_N2@P.

Solvent effects on the reaction PES

Now, we examine how solvation affects the shape of the PES of each reaction by decomposing the solution phase PES ($\Delta E_{solution}$) into two terms, namely, ΔE_{solute} and $\Delta E_{solvation}$ (see the Theoretical Methods section for details).[4e] The term ΔE_{solute} refers to the energy of the solute (computed in the gas phase, but with its solution-phase geometry), whereas $\Delta E_{solvation}$ is the stabilization provided by the solvent. Overall changes in the shape of the PES can be explained in terms of differential solvation of the various stationary points (i.e., R, RC, PC, pre-TS, post-TS, TS, and TC).[6] For nucleophilic substitutions involving an anionic nucleophile, such as the reactions studied in this work, it is known that a polar solvent stabilizes the reactants and products more strongly than the intermediate complexes that occur as the reaction progresses.[7b,d] Solvation, therefore, generally results in a destabilization of the region around the central transition state or transition complex.

This can be understood already from the classical electrostatic Born equation for spherical ions in a dielectric continuum [Eq. (4)] in combination with a simplified model of our S_N2 reaction systems.[28]

$$\Delta E_{solvation} = -\frac{Q^2}{8\pi\varepsilon_0 a}\left(1-\frac{1}{\varepsilon_r}\right) \quad (4)$$

In Equation (4), Q is the charge of the ion, a is the radius of the ion, ε_0 is the dielectric constant in vacuum, and ε_r is the relative dielectric constant of the solvent. The simplification involves the notion that the reaction systems consist of a relatively neutral central moiety (e.g., CH_3) between a (partially) negatively charged nucleophile Cl^1 and leaving group Cl^2. The latter two groups have charges Q_1 and Q_2 that, in the course of the S_N2 reaction, go from $Q_1 = -1$ and $Q_2 \cong 0$ to $Q_1 \cong 0$ and $Q_2 = -1$. This leads to the following Equation (5).

$$\Delta E_{solvation} = -\frac{{Q_1}^2+{Q_2}^2}{8\pi\varepsilon_0 a}\left(1-\frac{1}{\varepsilon_r}\right) \quad (5)$$

Equation (5) is, in fact, a crude approximation to the solvation energy as computed in our more sophisticated COSMO computations, but it catches the essence of the physics: solvation stabilization is strongest when the excess negative charge is localized mainly on one of the two ionic groups, that is, $Q_1 = -1$ or $Q_2 = -1$, and it is the least stabilizing in intermediate situations in which the charge is delocalized over both sides, that is, $Q_1 = Q_2 \cong -{}^1/_2$ [Eq. (5)]. As a result, the central part of the PES is less strongly stabilized compared to the reactant and product sides.

Striving to go one step beyond this general observation and explain how, and when, solvation can lead to PES shapes with different qualitative features (i.e., a labile TS or a stable TC, or the appearance of pre- and post-TSs), we have numerically recreated all occurring PES shapes by using generic Gaussian functions $f(x) = ae^{-x^2/b}$ (Figure 3). In each of the four graphs in Figure 3, an identical single-well ΔE_{solute} profile is represented by the solid black line. In addition, various $\Delta E_{solvation}$ profiles are modeled (colored dotted lines in Figure 3), by varying the peak width and peak height of the Gaussian functions. The colored solid lines are the sum of the modeled ΔE_{solute} profile and the $\Delta E_{solvation}$ model curves of the corresponding color, and represent the overall solution-phase PES profiles $\Delta E_{solution}$.

First, we discuss the effect of varying the peak width for the $\Delta E_{solvation}$ profiles. Our analysis reveals that when the ΔE_{solute} and $\Delta E_{solvation}$ profiles have roughly the same width, the resulting $\Delta E_{solution}$ PES will feature no stationary points other than the central TC or TS (red lines in Figure 3a). Due to the maximum of the $\Delta E_{solvation}$ curve in the middle, where it is the least stabilizing, the central point along the solution-phase PES $\Delta E_{solution}$ is destabilized relative to the central point along the solute PES ΔE_{solute} in vacuum. Whether this central point is a labile TS or stable TC also depends on the peak heights, which will be addressed hereafter. When the profile of $\Delta E_{solvation}$ is much wider than that of ΔE_{solute}, the solution-phase PES $\Delta E_{solution}$ [Eq. (2)] will develop pre-TS and post-TS barriers separating a central minimum or transition complex (TC) from the reactants and products. The reason is that near the reactants and products, the derivative $|d\Delta E_{solvation}/d\zeta| > |d\Delta E_{solute}/d\zeta|$, but nearer the central point $|d\Delta E_{solvation}/d\zeta| < |d\Delta E_{solute}/d\zeta|$. In other words, in early and late stages of the S_N2 reaction, $\Delta E_{solution}$ follows the destabilization of $\Delta E_{solvation}$ relative to the reactants and products, whereas, in the central region, it follows the stabilization, that is, the drop in energy stemming from ΔE_{solute}. This leads to the appearance of the aforementioned pre-TS and post-TS at points where the derivatives of ΔE_{solute} and $\Delta E_{solvation}$ are equal but of opposite sign: $d\Delta E_{solvation}/d\zeta = -d\Delta E_{solvation}/d\zeta$ (yellow lines in Figure 3a). A narrower $\Delta E_{solvation}$ profile, on the other hand, provides a labile central TS, with stable RC and PC (green lines in Figure 3a).

Now, turning to variation of the peak heights of the modeled $\Delta E_{solvation}$ profiles, we provide in Figure 3 a series of solvation energy profiles that have the same width as ΔE_{solute} (Figure 3b), are narrower than ΔE_{solute} (Figure 3c), or are wider than ΔE_{solute} (Figure 3d). For each situation, a small peak height does not lead to any change in the qualitative features of the solution phase $\Delta E_{solution}$ PES: the single well remains a single well (red lines in Figure 3b–d). A sufficiently large $\Delta E_{solvation}$ curve, does, however, change the single-well $\Delta E_{solution}$ PES to a unimodal profile with a central barrier (green lines in Figure 3b–d). When the peak heights of the ΔE_{solute} and $\Delta E_{solvation}$

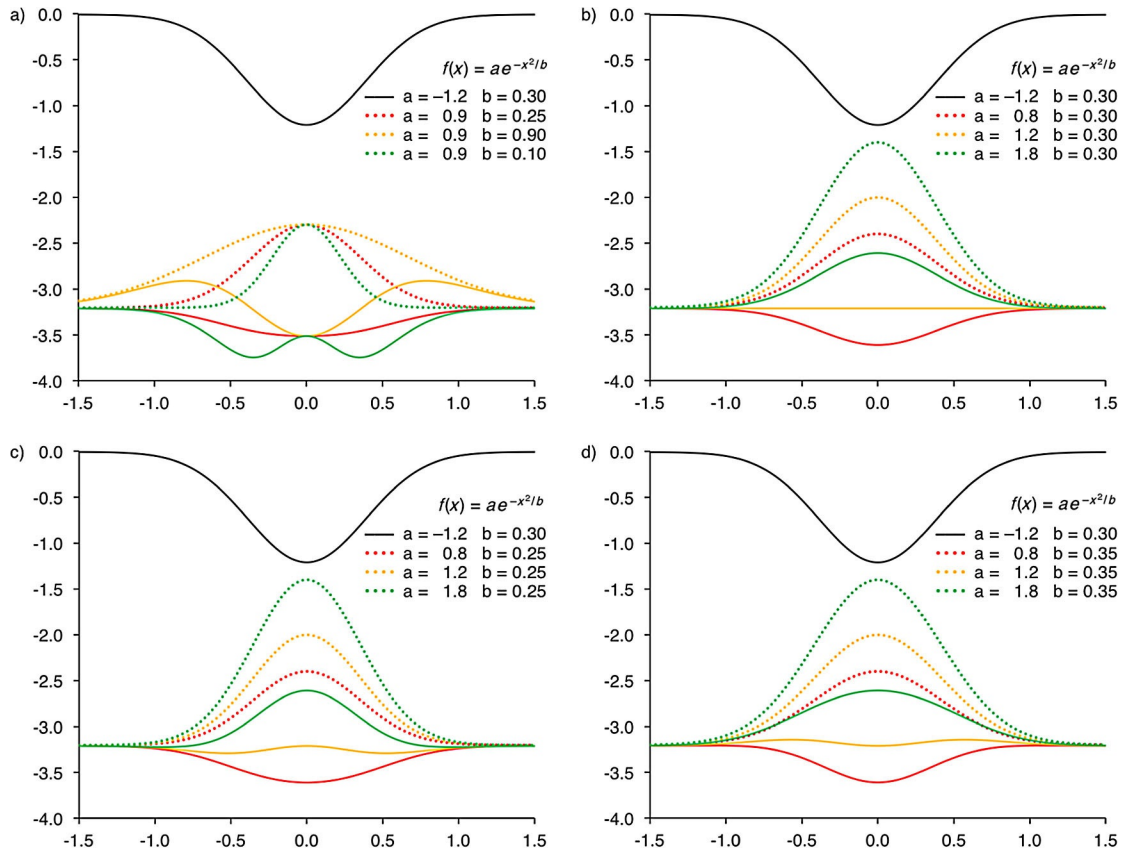

Figure 3. Analytical solution-phase PESs $\Delta E_{solution}$ (colored solid lines: $\Delta E_{solution} = \Delta E_{solute} + \Delta E_{solvation}$) based on generic Gaussian functions $f(x) = ae^{-x^2/b}$ to represent ΔE_{solute} (black solid lines: $a = -1.2$, $b = 0.30$) and $f(x) = ae^{-x^2/b} - 3.2$ to represent $\Delta E_{solvation}$ (colored dotted lines: shifted vertically by -3.2 to result in negative, that is, stabilizing, $\Delta E_{solvation}$ values; with various values for a and b). In all graphs, ΔE_{solute} is represented by the same Gaussian function, whereas the different $\Delta E_{solvation}$ profiles are obtained by varying the parameters a (peak height) and b (peak width). Graph a) shows the effect of varying peak width, graphs b), c), and d) show the effect of varying the peak height with the peak widths of $\Delta E_{solvation}$ chosen equal to, narrower than, and wider than that of ΔE_{solute}, respectively.

curves are comparable, the final reaction profile can contain stable RC and PC structures, separated by a TS (yellow lines in Figure 3c, $\Delta E_{solvation}$ peak width narrower than ΔE_{solute}), or the inverse situation can occur: the central point can be a stable minimum, with maxima appearing before and after, resembling a pre-TS and post-TS (yellow lines in Figure 3d, $\Delta E_{solvation}$ peak width broader than ΔE_{solute} peak width).

We now return to the actual chemical reactions that are investigated in this work. First, we recall that solvation raises the transition zone relative to the solvated reactants, for every S_N2 reaction included in this study. The total solvation energy for the reactants is dominated by the chloride ion with its localized charge: $\Delta E_{solvation}$ for this anion ranges from -45.3 to -77.9 kcal mol^{-1} from toluene to methylformamide, respectively (see Table 2, footnote [b]). The increased degree of stabilization (i.e., a more negative $\Delta E_{solvation}$) is directly correlated with the polarity of the solvent, with more polar solvent systems leading to amplified charge stabilization. Due to their lack of net charge, the neutral reactants are weakly solvated compared to Cl^-, ranging from -1.0 to -2.8 kcal mol^{-1} for non-oxide-based reactants (Table 2, entries 1a–h, 2a–h, 3a–h, 5a–h) and -5.1 to -12.8 kcal mol^{-1} for the more polar and moderately solvated tetracoordinate phosphorus and arsenic compounds (Table 2, Entries 4a–h, 6a–h). The RCs, pre-TSs, and central TCs/TSs display less strong solvation than the two separate reactants, with solvation energies ranging from -30.0 to -61.6 kcal mol^{-1}, and always becoming more stabilizing as the polarity of the solvent increases (Table 2). Overall, the difference in the stabilization between the reactants and the intermediate structures becomes greater for more polar solvents, thus leading to larger changes in the PES shapes. This is graphically shown in Figure 4a–c, where the ΔE_{solute}, $\Delta E_{solvation}$, and $\Delta E_{solution}$ terms are indicated for S_N2@P3 in toluene, ammonia, and methylformamide. For the apolar solvent toluene, we only find a minor change from the single-well PES for ΔE_{solute} to a shallower single-well PES for $\Delta E_{solution}$ (Figure 4a). Increasing the solvent polarity, as in the case of ammonia, we find that the single-well ΔE_{solute} curve is changed to a bimodal PES and even to a unimodal PES for the most polar solvent methylformamide (Figures 4b and c, respectively).

Next, we move to the effect of varying the central atom in the reaction system. We limit our discussion here to the results for the most polar solvent, namely methylformamide. For each reaction, we find a favorable solvation for the reactants, in all cases predominantly due to the Cl^- ion, which varies from -80.0 to -91.5 kcal mol^{-1} (Table 3). For S_N2@C, the $\Delta E_{solvation}$

Table 2. Solvation energies ($\Delta E_{solvation}$ in [kcal mol^{-1}]), chlorine atomic charges (Q_{Cl} in [a.u.]), and A–Cl distances (in [Å]) of the reactants, reactant complexes, pre-transition states, transition complexes, and transition states.[a]

No.	Medium[c]	Reaction	Reactants[b]			Reactant complex (or pre-transition state)			Transition state (or transition complex)		
			$\Delta E_{solvation}$	Q_{Cl}	A–Cl	$\Delta E_{solvation}$	Q_{Cl}	A–Cl	$\Delta E_{solvation}$	Q_{Cl}	A–Cl
1a	gas	$Cl^- + CH_3Cl$	–	−0.128	1.79	–	−0.225	1.83	–	−0.543	2.35
						–	−0.854	3.38			
1b	toluene		−1.0	−0.149	1.80	−40.6	−0.184	1.81	−33.0	−0.562	2.35
							−0.943	3.93			
1c	chloroform		−1.5	−0.160	1.80	−56.9	−0.175	1.80	−45.2	−0.570	2.35
							−0.965	4.23			
1d	ammonia		−1.8	−0.168	1.80	–	–	–	−53.9	−0.577	2.35
1e	methanol		−1.6	−0.169	1.80	–	–	–	−55.6	−0.578	2.35
1f	water		−1.8	−0.170	1.80	–	–	–	−56.2	−0.579	2.35
1g	formamide		−2.0	−0.170	1.80	–	–	–	−56.8	−0.579	2.35
1h	methylformamide		−2.0	−0.171	1.80	–	–	–	−57.0	−0.579	2.35
2a	gas	$Cl^- + SiH_3Cl$	–	−0.156	2.07	–	–	–	–	(−0.474)	(2.35)
2b	toluene		−1.1	−0.178	2.08	–	–	–	(−30.0)	(−0.492)	(2.36)
2c	chloroform		−1.6	−0.191	2.08	–	–	–	(−40.9)	(−0.501)	(2.37)
2d	ammonia		−2.2	−0.202	2.09	(−51.7)	(−0.370)	(2.21)	(−48.8)	(−0.507)	(2.38)
							(−0.678)	(2.69)			
2e	methanol		−2.3	−0.204	2.09	(−52.3)	(−0.393)	(2.23)	(−50.4)	(−0.509)	(2.38)
							(−0.647)	(2.62)			
2f	water		−2.2	−0.205	2.09	(−52.5)	(−0.403)	(2.25)	(−50.8)	(−0.509)	(2.38)
							(−0.635)	(2.59)			
2g	formamide		−2.3	−0.205	2.09	(−52.9)	(−0.410)	(2.26)	(−51.4)	(−0.510)	(2.38)
							(−0.625)	(2.57)			
2h	methylformamide		−2.3	−0.206	2.09	(−53.1)	(−0.410)	(2.26)	(−51.7)	(−0.510)	(2.38)
							(−0.626)	(2.57)			
3a	gas	$Cl^- + PH_2Cl$	–	−0.140	2.08	–	–	–	–	(−0.497)	(2.42)
3b	toluene		−1.1	−0.163	2.09	–	–	–	−30.4)	(−0.511)	(2.42)
3c	chloroform		−1.7	−0.175	2.09	–	–	–	(−41.6)	(−0.517)	(2.42)
3d	ammonia		−2.1	−0.184	2.10	(−61.3)	(−0.215)	(2.12)	(−49.5)	(−0.522)	(2.42)
							(−0.909)	(3.57)			
3e	methanol		−2.2	−0.187	2.10	(−61.6)	(−0.227)	(2.13)	(−51.1)	(−0.522)	(2.42)
							(−0.886)	(3.39)			
3f	water		−2.1	−0.188	2.10	–	–	–	−51.5	−0.523	2.42
3g	formamide		−2.3	−0.188	2.10	–	–	–	−52.2	−0.523	2.42
3h	methylformamide		−2.3	−0.188	2.10	–	–	–	−52.4	−0.523	2.42
4a	gas	$Cl^- + POH_2Cl$	–	−0.094	2.04	–	–	–	–	(−0.447)	(2.37)
4b	toluene		−5.1	−0.096	2.04	–	–	–	(−32.1)	(−0.468)	(2.36)
4c	chloroform		−7.4	−0.097	2.04	–	–	–	−44.4	−0.471	2.36
4d	ammonia		−9.4	−0.098	2.04	–	–	–	−53.4	−0.474	2.36
4e	methanol		−9.8	−0.098	2.04	–	–	–	−55.1	−0.474	2.36
4f	water		−9.9	−0.098	2.04	–	–	–	−55.8	−0.474	2.36
4g	formamide		−10.1	−0.098	2.04	–	–	–	−56.4	−0.474	2.36
4h	methylformamide		−10.1	−0.098	2.04	–	–	–	−56.6	−0.474	2.36
5a	gas	$Cl^- + AsH_2Cl$	–	−0.180	2.21	–	–	–	–	(−0.517)	(2.53)
5b	toluene		−1.3	−0.212	2.23	–	–	–	(−30.2)	(−0.534)	(2.54)
5c	chloroform		−2.0	−0.228	2.24	–	–	–	(−41.4)	(−0.541)	(2.54)
5d	ammonia		−2.6	−0.243	2.24	–	–	–	(−49.3)	(−0.547)	(2.54)
5e	methanol		−2.7	−0.246	2.25	–	–	–	(−50.9)	(−0.548)	(2.55)
5f	water		−2.6	−0.248	2.25	–	–	–	(−51.3)	(−0.548)	(2.55)
5g	formamide		−2.8	−0.248	2.25	–	–	–	(−52.0)	(−0.549)	(2.55)
5h	methylformamide		−2.8	−0.249	2.25	–	–	–	(−52.3)	(−0.549)	(2.55)

term becomes smaller during the reaction (−57.0 kcal mol^{-1} in the TS), combined with the high intrinsic barrier caused by steric congestion around the small carbon atom, this is enough to transform the double-well PES to a unimodal PES with a central barrier of +22.8 kcal mol^{-1}.

For S_N2@Si and S_N2@As4, solvation in methylformamide results in a bimodal PES (Figures 2b and f). From our results, we find a correlation between the slope of the solvation energy ($d\Delta E_{solvation}/d\zeta$, see Figure S2 in the Supporting Information) and the nature of the central atom: $d\Delta E_{solvation}/d\zeta$ becomes smaller, that is, the curve becomes less steep, as one moves down in the periodic table. This leads to a wider $\Delta E_{solvation}$ profile and consequently, the appearance of a pre-TS and post-TS (see Figure 3d). Why the $\Delta E_{solvation}$ profile becomes broader for larger central atoms, can be understood from an examination of the various AR_nCl fragments (see Figures S3 and S4 in the Supporting Information). The LUMO of AR_nCl grows progressively more diffuse as one moves down in the periodic table

Table 2. (Continued)

No.	Medium[c]	Reaction	Reactants[b]			Reactant complex (or pre-transition state)			Transition state (or transition complex)		
			$\Delta E_{solvation}$	Q_{Cl}	A–Cl	$\Delta E_{solvation}$	Q_{Cl}	A–Cl	$\Delta E_{solvation}$	Q_{Cl}	A–Cl
6a	gas	$Cl^- + AsOH_2Cl$	–	−0.142	2.19	–	–	–	–	(−0.475)	(2.48)
6b	toluene		−6.2	−0.152	2.19	–	–	–	(−32.8)	(−0.485)	(2.47)
6c	chloroform		−9.3	−0.157	2.19	–	–	–	(−45.6)	(−0.489)	(2.47)
6d	ammonia		−11.8	−0.160	2.19	(−57.8)	(−0.327)	(2.30)	(−55.0)	(−0.492)	(2.47)
							(−0.688)	(2.80)			
6e	methanol		−12.3	−0.161	2.19	(−58.3)	(−0.372)	(2.34)	(−56.8)	(−0.492)	(2.47)
							(−0.629)	(2.68)			
6f	water		−12.6	−0.161	2.19	(−58.6)	(−0.393)	(2.36)	(−57.6)	(−0.492)	(2.47)
							(−0.603)	(2.63)			
6g	formamide		−12.8	−0.161	2.19	(−58.8)	(−0.424)	(2.39)	(−58.2)	(−0.493)	(2.47)
							(−0.567)	(2.57)			
6h	methylformamide		−12.8	−0.161	2.19	(−59.0)	(−0.414)	(2.38)	(−58.5)	(−0.493)	(2.47)
							(−0.578)	(2.59)			

[a] Computed at the OLYP/TZ2P level. Q_{Cl} values obtained in the corresponding medium with the Voronoi deformation density (VDD) method presented in [a.u.][27] (when two values are given, the top and bottom values are for the LG and the Nu, respectively). [b] Values refer to the substrate. $\Delta E_{solvation}$ for Cl^- is −45.3, −61.9, −73.7, −76.0, −76.6, −77.7, and −77.9 kcal mol^{-1}, in toluene, chloroform, ammonia, methanol, water, formamide, and methylformamide, respectively. [c] Modeled with COSMO.

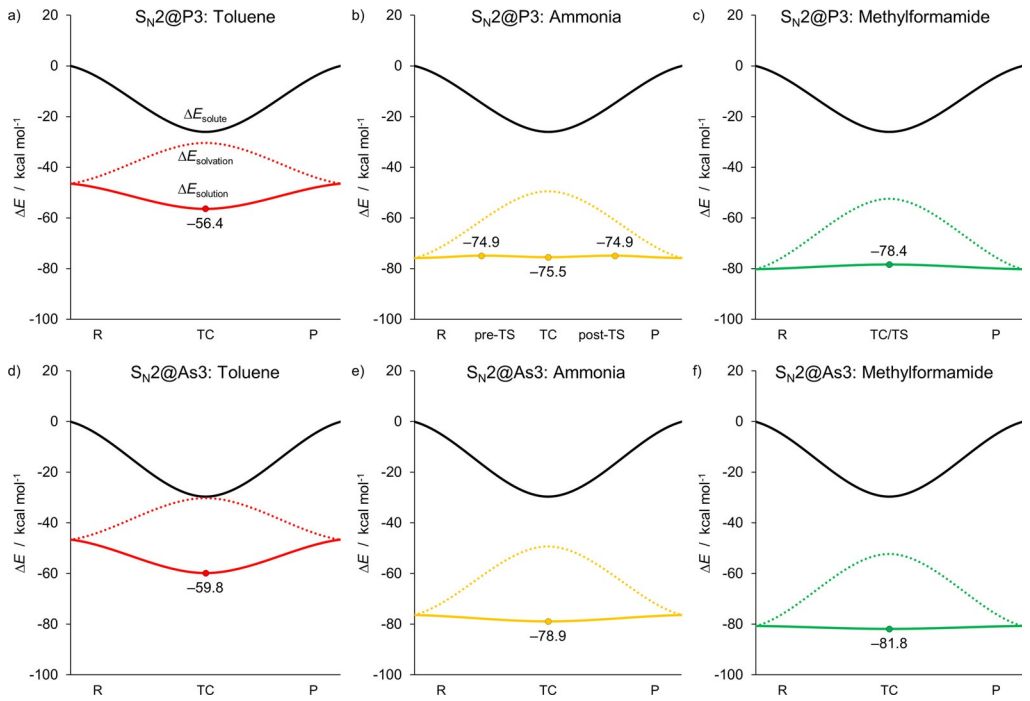

Figure 4. Solvent effects on the PESs for a,b,c) S$_N$2@P3 and d,e,f) S$_N$2@As4 reaction in solvents of varying polarity: toluene (a and d), ammonia (b and e), and methylformamide (c and f). As described in Equation (2), the $\Delta E_{solution}$ term (solution: colored solid curves) is comprised of the ΔE_{solute} term (solute: black solid curves) and the $\Delta E_{solvation}$ term (solvation: colored dotted curves).

(i.e., C to Si, P to As). This trend in the size of the LUMO coincides nicely with the electronegativity of the central atoms, with the larger, less electronegative ones (Si and As) displaying a relatively diffuse LUMO. A more diffuse LUMO (i.e., a relatively large amplitude at large distance from the central atom) allows for both charge transfer and $HOMO_{Cl^-}/LUMO_{AR_nCl}$ overlap to develop in a more gradual fashion along the reaction coordinate ζ, and thus, a wider $\Delta E_{solvation}$ profile. This situation is schematically indicated by the red lines in Figure 5: an earlier, more gradual charge transfer from the nucleophile to the substrate leads to smaller values of $\Sigma(Q_{Cl}^2)$ at an earlier stage during the reaction, and, as also follows from an approximation based on the Born equation [Eq. (4)],[27] to an earlier rise (i.e., becoming less stabilizing) of the solvation energy profile $\Delta E_{solvation}$. Analysis of the chloride Voronoi deformation density (VDD) charges (Q_{Cl}) along the various PESs confirms that as the LUMO becomes larger, the chloride charge delocalizes indeed in a more gradual manner (similar trends emerge if instead we use, e.g., Hirshfeld charges, see Figure S5 in the Supporting Information).

Table 3. Relative energies in solution ($\Delta E_{solution}$), solvation energies ($\Delta E_{solvation}$), and solute energies (ΔE_{solute}) (all in [kcal mol^{-1}], relative to the gas-phase reactants) in methylformamide.[a]

No.	Reaction	Reactants[b]			Reactant complex/(pre-transition state)			Transition state/(transition complex)		
		$\Delta E_{solution}$	$\Delta E_{solvation}$	ΔE_{solute}[c]	$\Delta E_{solution}$	$\Delta E_{solvation}$	ΔE_{solute}	$\Delta E_{solution}$	$\Delta E_{solvation}$	ΔE_{solute}
1 h	Cl^-+CH_3Cl	−80.0	−80.0	0.0	–	–	–	−57.2	−57.0	−0.2
2 h	Cl^-+SiH_3Cl	−80.5	−80.5	0.0	(−76.0)	(−53.1)	(−22.9)	(−76.1)	(−51.7)	(−24.4)
3 h	Cl^-+PH_2Cl	−80.3	−80.3	0.0	–	–	–	−78.4	−52.3	−26.1
4 h	Cl^-+POH_2Cl	−88.5	−88.5	0.0	–	–	–	−78.8	−56.6	−22.2
5 h	Cl^-+AsH_2Cl	−81.0	−81.0	0.0	–	–	–	(−82.1)	(−52.3)	(−29.8)
6h	Cl^-+AsOH_2Cl	−91.5	−91.5	0.0	(−87.9)	(−59.0)	(−28.9)	(−88.0)	(−58.5)	(−29.5)

[a] Energies computed at the OLYP/TZ2P level. [b] Comprises both Cl^- and the substrate. [c] Value set to 0.0 kcal mol^{-1}.

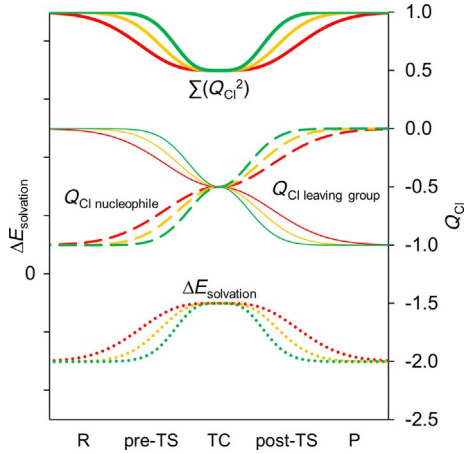

Figure 5. Qualitative relationship between the rate at which the charges of the chlorides (Q_{Cl}, nucleophile = dashed curve, leaving group = solid curve) change along the reaction coordinate and, through the sum of Q_{Cl}^2, effect on the solvation energy term.

Examination of the Mulliken gross population of the LUMOs of AR_nCl (see Figure S4 in the Supporting Information) further supports this relationship between the size of the LUMO and charge transfer. It is important to note that for S_N2@As3 a single-well PES persists in all solvents, because, due to the large LUMO and the strong stability of the central TC, the PES is virtually resistant towards solvation-induced changes (Figures 4 d–f). And conversely, a more compact LUMO (as observed for small central atoms, such as in S_N2@C and S_N2@P) is associated with a delayed but fast charge transfer that occurs in the proximity of the transition structure. Such a situation leads to a narrow $\Delta E_{solvation}$ profile, as indicated by green lines in Figure 5, and is more likely to convert a stable TC into a TS.

Activation strain analysis

Lastly, an activation strain analysis (ASA) on the solute, ΔE_{solute}, (i.e., the reaction system in solution, but with the solvent taken away) transition structure (either TS or TC) for each of the S_N2 reactions is presented. Decomposing the ΔE_{solute} term into the ΔE_{strain} and ΔE_{int} terms, yields insight into how the barrier or well arises.[4e] Results from the ASA are collected in Table 4.

Table 4. Activation strain analysis (in [kcal mol^{-1}]) of the solute (optimized in methylformamide) in the gas phase for all studied S_N2 reactions.

No.	Reaction	Transition state (transition complex)		
		ΔE_{strain}	ΔE_{int}	ΔE_{solute}
1	Cl^-+CH_3Cl	31.6	−31.8	−0.2
2	Cl^-+SiH_3Cl	(25.2)	(−49.5)	(−24.4)
3	Cl^-+PH_2Cl	(13.4)	(−39.4)	(−26.1)
4	Cl^-+POH_2Cl	(26.9)	(−49.1)	(−22.3)
5	Cl^-+AsH_2Cl	(11.0)	(−40.8)	(−29.8)
6	Cl^-+AsOH_2Cl	(20.4)	(−50.0)	(−29.6)

[a] Computed at the OLYP/TZ2P level.

First, we analyze the S_N2@C reaction Cl^-+CH_3Cl (Table 4, entry 1). The transition state marks the top of a central barrier that connects reactant and product complexes. Note, however, that ΔE_{solute}(TS) is below the separate reactants by −0.2 kcal mol^{-1}. This is because the initial interaction energy is very favorable. This leads to the occurrence of rather stable reactant complexes from which the actual substitution process proceeds. In general, this can but does not have to lead to pronouncedly negative overall barriers.[4j] In the present case, there is near cancellation of the favorable interaction energy between the nucleophile and the substrate by the strain energy required to distort the CH_3Cl to the geometry it adopts in the TS.

The stabilizing nucleophile–substrate interaction is much stronger for S_N2@Si ($\Delta\Delta E_{int} = -17.7$ kcal mol^{-1}), whereas the strain energy is decreased compared to S_N2@C ($\Delta\Delta E_{strain} = -6.4$ kcal mol^{-1}). These are direct results of the decreased steric congestion at the silicon atom (i.e., all bonds are elongated in SiH_3Cl compared to CH_3Cl).[7b] The combination of a greater ΔE_{int} and a reduced ΔE_{strain} result in a single-well, with a pronouncedly stable TC instead of a central barrier for S_N2@Si (Table 4, entry 2).

The ΔE_{strain} for S_N2@P3 amounts to +13.4 kcal mol^{-1} and is thus lower compared to S_N2@C (+31.6 kcal mol^{-1}) and S_N2@Si (+25.2 kcal mol^{-1}) reactions. This is due to the decreased coordination of the phosphorous atom.[8f] The ΔE_{int} (−39.4 kcal mol^{-1}) is three times greater (in absolute terms) than ΔE_{strain}, thus resulting in a deep single-well PES ($\Delta E_{solute} = -26.1$ kcal mol^{-1}). Increasing the coordination at the phosphorus (POH_2Cl) for S_N2@P4 directly doubles the strain energy (+26.9 kcal

mol^{-1}) of the TC. The ΔE_{int} is also enhanced and is more favorable than for trivalent phosphorus ($\Delta\Delta E_{int} = -9.7$ kcal mol^{-1}). The more favorable interaction energy results in a single-well that is -22.3 kcal mol^{-1} below the reactants.

The depths of the single-well PESs for the S_N2@As3 and S_N2@As4 reactions are nearly equivalent, with a ΔE_{solute} of -29.8 and -29.6 kcal mol^{-1}, respectively. Nonetheless, the ΔE_{strain} and ΔE_{int} follow similar trends as previously described for the S_N2@P3 and S_N2@P4 reactions, specifically the ΔE_{strain} in the $[Cl\text{-}AsOH_2\text{-}Cl]^-$ TC is double that of the tricoordinate TC and the interaction is more favorable. Comparing S_N2@As4 to S_N2@As3, we see the energetic penalty associated with the strain term ($\Delta\Delta E_{strain} = 9.4$ kcal mol^{-1}) is completely negated by the more favorable interaction energy ($\Delta\Delta E_{int} = -9.2$ kcal mol^{-1}).

The above analyses demonstrate how the interplay of strain and interaction energies determines the course and barrier height/well depth of the solute in these S_N2 reactions. They suggest that by either decreasing the steric congestion at the central atom, or by strengthening the nucleophile–substrate interaction in the solute, the S_N2 barrier can disappear. This is what happens when moving from $Cl^- + CH_3Cl$ to S_N2@Si, S_N2@P3, S_N2@P4, S_N2@As3, and S_N2@As4 reactions. The solute TS turns into a stable TC because the strain energy associated with reaching the transition structure is decreased and the interaction energy is enhanced significantly. Furthermore, by comparing S_N2@P3 with S_N2@P4 and S_N2@As3 with S_N2@As4, we see that the extra oxygen substituent results in extra steric congestion, yet the penalty associated with strain is compensated by increased favorable interactions.

Conclusion

Solvation can dramatically modify not only the rate of S_N2 substitutions, but also the shape of their reaction potential energy surface and, thus, the nature of this reaction mechanism. The effect strongly depends on the polarity of the solvent and the type of the S_N2 system, as follows from our DFT study of six anionic model S_N2 reactions, $Cl^- + AR_nCl$, at various Group 14 (C, Si) and Group 15 (P, As) electrophilic centers, each modeled in the gas phase as well as seven solvents of varying polarity.

General trends can be gleaned from our results, in that all barriers increase in a monotonic fashion as the solvent polarity increases. In the gas phase, all but the S_N2@C model substitutions proceed through a single-well PES without a TS, whereas the former, that is, S_N2@C shows the known double-well potential. In the limit of strong solvation, the PES becomes eventually unimodal for the S_N2@C, S_N2@P3, and S_N2@P4 reactions and bimodal for the S_N2@Si and S_N2@As4 reactions. The gas-phase single-well PES for S_N2@P3 transforms into a bimodal reaction profile in ammonia, before it shifts to a unimodal barrier in methanol and increasingly polar solvents. All solvent effects, not only the raise in the barrier but also the transformation of the PES shapes can be understood in terms of differential solvation, that is, the stronger solvation stabilization of reactants and products (especially Cl^-, but also reactant and product complexes) and weaker solvation stabilization of hypercoordinate intermediates (e.g., $[Cl\text{-}AsH_2\text{-}Cl]^-$) or transition states (e.g., $[Cl\text{-}CH_3\text{-}Cl]^{-\ddagger}$).

The size or spatial distribution of the LUMO on the AR_nCl substrate controls the width (and shallowness) of the solvation energy profile $\Delta E_{solvation}$: this orbital determines how early and gradual, or late and abrupt, charge flows from the nucleophile to the leaving group. Diffuse LUMOs, as present on substrates with heavier central atoms, allow for an earlier and more gradual charge delocalization. Delocalization of charge at an early stage of the reaction, results, in accordance with the Born equation, in a wide $\Delta E_{solvation}$ profile, whereas more abrupt delocalization, occurring only closely around the central point of the reaction, results in a narrow $\Delta E_{solvation}$ profile. These principles can lead to the following situations for a single-well ΔE_{solute}, a curve with one minimum, and the unimodal $\Delta E_{solvation}$, a curve with one maximum: 1) a combination of a narrow ΔE_{solute} profile and a broad $\Delta E_{solvation}$ profile is likely to provide a PES with a pre-TS and post-TS surrounding a stable minimum; 2) a combination of a broad ΔE_{solute} profile and a narrow $\Delta E_{solvation}$ profile more often leads to a central TS; and 3) when the ΔE_{solute} and $\Delta E_{solvation}$ profiles have similar widths, the transition region contains either a TC or a TS (no other stationary points), determined by the height of the $\Delta E_{solvation}$ curve. For example, solvation of S_N2@C and S_N2@P (relatively compact LUMOs on the central atom) is more likely to result in a solution-phase PES with a central TS. On the other hand, solvation of S_N2@Si and S_N2@As (relatively diffuse LUMOs on the central atom) tends to provide a stable central TC, which may be flanked by a pre- and post-TS depending on the height of the $\Delta E_{solvation}$ profile.

Acknowledgements

We thank the Netherlands Organization for Scientific Research (NWO) for financial support through the Planetary and Exo-Planetary Science program (PEPSci) and the Dutch Astrochemistry Network (DAN). We also thank SURFsara for generous allocation of computational resources. Prof. Dr. Jordi Poater of the Universitat de Barcelona and Prof. Dr. Christian S. Hamann of the Albright College are thanked for helpful discussions throughout the course of this project.

Conflict of interest

The authors declare no conflict of interest.

Keywords: density functional calculations · nucleophilic substitution · potential energy surfaces · reaction mechanisms · solvent effects

[1] a) M. B. Smith, *March's Advanced Organic Chemistry: Reactions, Mechanisms and Structure*, 7th ed. Wiley, New York, **2013**; b) F. A. Carey, R. J. Sundberg, *Advanced Organic Chemistry, Part A*, Plenum Press, New York, **1984**; c) C. K. Ingold, *Structure and Mechanism in Organic Chemistry*, Cornell University Press, Ithaca, NY, **1969**.

[2] a) T. A. Hamlin, M. Swart, F. M. Bickelhaupt, *ChemPhysChem* **2018**, https://doi.org/10.1002/cph.201701363; b) E. Uggerud, *Adv. Phys. Org. Chem.* **2017**, *51*, 1 – 57.

[3] a) M. Peifer, R. Berger, V. W. Shurtleff, J. C. Conrad, D. W. C. MacMillan, *J. Am. Chem. Soc.* **2014**, *136*, 5900 – 5903; b) T. A. Hamlin, C. B. Kelly, R. M. Cywar, N. E. Leadbeater, *J. Org. Chem.* **2014**, *79*, 1145 – 1155; c) T. A. Hamlin, C. B. Kelly, N. E. Leadbeater, *Eur. J. Org. Chem.* **2013**, 3658 – 3661; d) R. Kretschmer, M. Schlange, H. Schwarz, *Angew. Chem. Int. Ed.* **2011**, *50*, 5387 – 5391; *Angew. Chem.* **2011**, *123*, 5499 – 5503; e) J. M. Garver, S. Gronert, V. M. Bierbaum, *J. Am. Chem. Soc.* **2011**, *133*, 13894 – 13897; f) J. M. Garver, Y, Fang, N. Eyet, S. M. Villano, V. M. Bierbaum, K. C. Westaway, *J. Am. Chem. Soc.* **2010**, *132*, 3808 – 3814; g) J. Mikosch, S. Trippel, C. Eichhorn, R. Otto, U. Lourderaj, J. X. Zhang, W. L. Hase, M. Weidemüller, R. Wester, *Science* **2008**, *319*, 183 – 186.

[4] a) M. J. Ryding, I. Fernández, E. Uggerud, *Phys. Chem. Chem. Phys.* **2017**, *19*, 23176 – 23186; b) J. Kubelka, F. M. Bickelhaupt, *J. Phys. Chem. A* **2017**, *121*, 885 – 891; c) M. Stei, E. Carrascosa, M. A. Kainz, A. H. Kelkar, J. Meyer, I. Szabó, G. Czakó, R. Wester, *Nat. Chem.* **2016**, *8*, 151 – 156; d) J. Xie, W. L. Hase, *Science* **2016**, *352*, 32 – 33; e) J. Z. A. Laloo, L. Rhyman, P. Ramasami, F. M. Bickelhaupt, A. de Cózar, *Chem. Eur. J.* **2016**, *22*, 4431 – 4439; f) I. Szabó, G. Czakó, *Nat. Commun.* **2015**, *6*, 5972 – 5978; g) M. J. Ryding, A. Debnárová, I. Fernández, E. Uggerud, *J. Org. Chem.* **2015**, *80*, 6133 – 6142; h) J. Xie, R. Otto, J. Mikosch, J. Zhang, R. Wester, W. L. Hase, *Acc. Chem. Res.* **2014**, *47*, 2960 – 2969; i) L. P. Wolters, Y. Ren, F. M. Bickelhaupt, *ChemistryOpen* **2014**, *3*, 29 – 36; j) A. P. Bento, F. M. Bickelhaupt, *J. Org. Chem.* **2008**, *73*, 7290 – 7299; k) E. Uggerud, *J. Chem. Soc. Perkin Trans. 2* **1999**, 1465 – 1467; l) L. Q. Deng, V. Branchadell, T. Ziegler, *J. Am. Chem. Soc.* **1994**, *116*, 10645 – 10656; m) J. Chandrasekhar, W. L. Jorgensen, *J. Am. Chem. Soc.* **1985**, *107*, 2974 – 2975; n) A. P. Bento, M. Solà, F. M. Bickelhaupt, *J. Chem. Theory Comput.* **2008**, *4*, 929 – 940.

[5] a) E. R. Kuechler, D. M. York, *J. Chem. Phys.* **2014**, *140*, 054109; b) D. K. Bohme, A. B. Rakshit, G. L. Mackay, *J. Am. Chem. Soc.* **1982**, *104*, 1100 – 1101; c) D. K. Bohme, G. I. Mackay, *J. Am. Chem. Soc.* **1981**, *103*, 978 – 979; d) A. J. Parker, *Chem. Rev.* **1969**, *69*, 1 – 32.

[6] G. Schreckenbach, *Chem. Eur. J.* **2017**, *23*, 3797 – 3803.

[7] a) N. Laskowski, E.-M. Reis, L. Kötzner, J. A. Baus, C. Burschka, R. Tacke, *Organometallics* **2013**, *32*, 3269 – 3278; b) M. A. van Bochove, F. M. Bickelhaupt, *Eur. J. Org. Chem.* **2008**, 649 – 654; c) A. P. Bento, M. Solà, F. M. Bickelhaupt, *J. Comput. Chem.* **2005**, *26*, 1497 – 1504; d) C. Reichardt, *Solvents and Solvent Effects in Organic Chemistry*, 3rd ed., Wiley-VCH, Weinheim, **2003**; e) R. R. Holmes, *Chem. Rev.* **1996**, *96*, 927 – 950; f) T. L. Windus, M. S. Gordon, L. P. Davis, L. W. Burggraf, *J. Am. Chem. Soc.* **1994**, *116*, 3568 – 3579; g) S. Gronert, R. Glaser, A. Streitwieser, *J. Am. Chem. Soc.* **1989**, *111*, 3111 – 3117; h) R. Damrauer, L. W. Burggraf, L. P. Davis, M. S. Gordon, *J. Am. Chem. Soc.* **1988**, *110*, 6601 – 6606.

[8] a) K. Nikitin, E. V. Jennings, S. A. Sulaimi, Y. Ortin, D. G. Gilheany, *Angew. Chem. Int. Ed.* **2018**, *57*, 1480 – 1484; *Angew. Chem.* **2018**, *130*, 1496 – 1500 ; b) L.-J. Liu, W.-M. Wang, L. Yao, F.-J. Meng, Y.-M. Sun, H. Xu, Z.-Y. Xu, Q. Li, C.-Q. Zhao, L.-B. Han, *J. Org. Chem.* **2017**, *82*, 11990 – 12002; c) E. V. Jennings, K. Nikitin, Y. Ortin, D. G. Gilheany, *J. Am. Chem. Soc.* **2014**, *136*, 16217 – 16226; d) A. J. M. Ribeiro, M. J. Ramos, P. A. Fernandes, *J. Chem. Theory Comput.* **2010**, *6*, 2281 – 2292; e) M. A. van Bochove, M. Swart, F. M. Bickelhaupt, *ChemPhysChem* **2007**, *8*, 2452 – 2463; f) M. A. van Bochove, M. Swart, F. M. Bickelhaupt, *J. Am. Chem. Soc.* **2006**, *128*, 10738 – 10744; g) C. Fish, M. Green, R. J. Kilby, J. M. Lynam, J. E. McGrady, D. A. Pantazis, C. A. Russell, A. C. Whitwood, C. E. Willans, *Angew. Chem. Int. Ed.* **2006**, *45*, 3628 – 3631; *Angew. Chem.* **2006**, *118*, 3710 – 3713; h) K. C. Kumara Swamy, N. Satish Kumar, *Acc. Chem. Res.* **2006**, *39*, 324 – 333; i) R. R. Holmes, *Acc. Chem. Res.* **2004**, *37*, 746 – 753; j) K. Range, M. J. McGrath, X. Lopez, D. M. York, *J. Am. Chem. Soc.* **2004**, *126*, 1654 – 1665; k) C. Lim, M. Karplus, *J. Am. Chem. Soc.* **1990**, *112*, 5872 – 5873.

[9] *CRC Handbook of Chemistry and Physics*, 90th ed. (Internet Version 2010) (Ed.: D. Lide), CRC Press/Taylor & Francis, Boca Raton, FL, **2010**.

[10] a) F. Wolfe-Simon, P. C. W. Davies, A. D. Anbar, *Int. J. Astrobiol.* **2009**, *8*, 69 – 74; b) R. A. Kohn, T. F. Dunlap, *J. Anim. Sci.* **1998**, *76*, 1702 – 1709; c) M. M. Kish, R. E. Viola, *Inorg. Chem.* **1999**, *38*, 818 – 820; d) E. H. Larsen, S. H. Hansen, *Microchim. Acta* **1992**, *109*, 47 – 51.

[11] F. Wolfe-Simon, J. S. Blum, T. R. Kulp, G. W. Gordon, S. E. Hoeft, J. Pett-Ridge, J. F. Stolz, S. M. Webb, P. K. Weber, P. C. W. Davies, A. D. Anbar, R. S. Oremland, *Science* **2011**, *332*, 1163 – 1166.

[12] a) T. J. Erb, P. Kiefer, B. Hattendorf, D. Günther, J. A. Vorholt, *Science* **2012**, *337*, 467 – 470; b) M. L. Reaves, S. Sinha, J. D. Rabinowitz, L. Kruglyak, R. J. Redfield, *Science* **2012**, *337*, 470 – 473; c) M. Elias, A. Wellner, K. Goldin-Azulay, E. Chabriere, J. A. Vorholt, T. J. Erb, D. S. Tawfik, *Nature* **2012**, *491*, 134 – 137.

[13] A. Mládek, J. Šponer, B. G. Sumpter, M. Fuentes-Cabrera, J. E. Šponer, *Phys. Chem. Chem. Phys.* **2011**, *13*, 10869 – 10871.

[14] a) M. A. van Bochove, G. Roos, C. Fonseca Guerra, T. A. Hamlin, F. M. Bickelhaupt, *Chem. Commun.* **2018**, *54*, https://dx.doi.org/10.1039/C8CC00700D; b) T. A. Hamlin, J. Poater, C. Fonseca Guerra, F. M. Bickelhaupt, *Phys. Chem. Chem. Phys.* **2017**, *19*, 16969 – 16978.

[15] a) C. C. Porco, P. Helfenstein, P. C. Thomas, A. P. Ingersoll, J. Wisdom, R. West, G. Neukum, T. Denk, R. Wagner, T. Roatsch, S. Kieffer, E. Turtle, A. McEwen, T. V. Johnson, J. Rathbun, J. Veverka, D. Wilson, J. Perry, J. Spitale, A. Brahic, J. A. Burns, A. D. DelGenio, L. Dones, C. D. Murray, S. Squyres, *Science* **2006**, *311*, 1393 – 1401; b) R. Hueso, A. Sánchez-Lavega, *Nat. Lett.* **2006**, *442*, 428 – 431; c) C. P. McKay, H. D. Smith, *Icarus* **2005**, *178*, 274 – 276; d) D. C. Jewitt, J. Luu, *Nature* **2004**, *432*, 731 – 733; e) J. M. Bauer, R. L. Roush, T. R. Geballe, K. J. Meech, T. C. Owen, W. D. Vacca, J. T. Rayner, K. T. C. Jim, *Icarus* **2002**, *158*, 178 – 190; f) E. J. Gaidos, F. Nimmo, *Nature* **2000**, *405*, 637; g) D. Stevenson, *Science* **2000**, *289*, 1305 – 1307; h) M. E. Brown, W. M. Calvin, *Science* **2000**, *287*, 107 – 109; i) W. B. Hubbard, *Science* **1981**, *214*, 145 – 149.

[16] a) R. G. Parr, W. Yang, *Density Functional Theory of Atoms and Molecules*, Oxford University Press, New York, **1989**; b) W. Koch, M. C. Holthausen, *A Chemist's Guide to Density Functional Theory*, Wiley-VCH, Weinheim, **2000**; c) R. Dreizler, E. Gross, *Density Functional Theory*, Plenum Press, New York, **1995**; d) F. M. Bickelhaupt, E. J. Baerends, *Rev. Comput. Chem.* **2000**, *15*, 1 – 86; e) E. J. Baerends, O. V. Gritsenko, *J. Phys. Chem. A* **1997**, *101*, 5383 – 5403; f) T. Ziegler, *Can. J. Chem.* **1995**, *73*, 743 – 761; g) T. Ziegler, *Chem. Rev.* **1991**, *91*, 651 – 667.

[17] a) G. te Velde, F. M. Bickelhaupt, E. J. Baerends, C. Fonseca Guerra, S. J. A. van Gisbergen, J. G. Snijders, T. Ziegler, *J. Comput. Chem.* **2001**, *22*, 931 – 967; b) C. Fonseca Guerra, J. G. Snijders, G. te Velde, E. J. Baerends, *Theor. Chem. Acc.* **1998**, *99*, 391 – 403; c) ADF, SCM Theoretical Chemistry, Vrije Universiteit: Amsterdam (The Netherlands), **2016**, http://www.scm.com.

[18] a) N. C. Handy, A. J. Cohen, *J. Chem. Phys.* **2002**, *116*, 5411 – 5418; b) N. C. Handy, A. J. Cohen, *Mol. Phys.* **2001**, *99*, 403 – 412.

[19] C. T. Lee, W. T. Yang, R. G. Parr, *Phys. Rev. B* **1988**, *37*, 785 – 789.

[20] a) A. D. Becke, *J. Chem. Phys.* **1988**, *88*, 2547; b) M. Franchini, P. H. T. Philipsen, L. Visscher, *J. Comput. Chem.* **2013**, *34*, 1819 – 1827.

[21] a) A. Klamt, G. Schüürmann, *J. Chem. Soc. Perkin Trans. 2* **1993**, 799 – 805; b) A. Klamt, *J. Phys. Chem.* **1995**, *99*, 2224 – 2235; c) A. Klamt, V. Jonas, *J. Chem. Phys.* **1996**, *105*, 9972 – 9981; d) C. C. Pye, T. Ziegler, *Theor. Chem. Acc.* **1999**, *101*, 396 – 408.

[22] N. L. Allinger, X. Zhou, J. Bergsma, *J. Mol. Struct.* **1994**, *312*, 69 – 83.

[23] a) J. L. Pascual-Ahuir, E. Silla, I. Tunon, *J. Comput. Chem.* **1994**, *15*, 1127 – 1138; b) E. Silla, I. Tunon, J. L. Pascual-Ahuir, *J. Comput. Chem.* **1991**, *12*, 1077 – 1088; c) J. L. Pascual-Ahuir, E. Silla, *J. Comput. Chem.* **1990**, *11*, 1047 – 1060.

[24] Y. Marcus, *Biophys. Chem.* **1994**, *51*, 111 – 127.

[25] a) F. M. Bickelhaupt, K. N. Houk, *Angew. Chem. Int. Ed.* **2017**, *56*, 10070 – 10086; *Angew. Chem.* **2017**, *129*, 10204 – 10221; b) L. P. Wolters, F. M. Bickelhaupt, *WIRES Comput. Mol. Sci.* **2015**, *5*, 324 – 343; c) I. Fernández, F. M. Bickelhaupt, *Chem. Soc. Rev.* **2014**, *43*, 4953 – 4967; d) W.-J. van Zeist, F. M. Bickelhaupt, *Org. Biomol. Chem.* **2010**, *8*, 3118 – 3127; e) D. H. Ess, K. N. Houk, *J. Am. Chem. Soc.* **2008**, *130*, 10187 – 10198; f) D. H. Ess, G. O. Jones, K. N. Houk, *Org. Lett.* **2008**, *10*, 1633 – 1636; g) D. H. Ess, K. N. Houk, *J. Am. Chem. Soc.* **2007**, *129*, 10646 – 10647.

[26] G. T. de Jong, F. M. Bickelhaupt, *J. Chem. Theory Comput.* **2007**, *3*, 514 – 529.

[27] C. Fonseca Guerra, J. Handgraaf, E. J. Baerends, F. M. Bickelhaupt, *J. Comput. Chem.* **2004**, *25*, 189 – 210.

[28] M. Born, *Z. Phys.* **1920**, *1*, 45 – 48.

Manuscript received: December 21, 2017

Accepted manuscript online: February 19, 2018

Version of record online: March 22, 2018

